Computational Simulation of Wind Loads on Three Curved Eave Models with Different Height-Width Relationships

GUILHERME S. TEIXEIRA, LEONARDO G. TEODORO JÚNIOR, MARCO D. CAMPOS
Institute of Exact and Earth Sciences,
Federal University of Mato Grosso,
Av. Valdon Varjão, 6390, Barra do Garças, 78605-091, Mato Grosso,
BRAZIL

Abstract: - This work deals with the effects of wind loads on two industrial shed models with curved eaves aspect of different height-to-width ratios. Using *Ansys Workbench* software, the external pressure coefficients for the entire roof by applying refinement levels were determined. Also were studied the quality of the unstructured and tetrahedral grid according to recommendations to ensure greater efficiency in the simulation results. The results generated provided evidence that the wind in the transverse direction is more damaging in the windward region: for a wind at 45º the most critical region appeared both windward and leeward in the model with a ratio of h/b=0.5 (*Model 1*) and to windward in the models with a ratio of h/b=1 (*Model 2*) and h/b=1.5 (*Model 3*). The leeward suctions increased due to the reduction in the height-width ratio considering a wind direction of 45º. The increase in this ratio intensified the values of the external pressure coefficients in the windward region for the 90º wind direction.

Key-Words: - Wind action, industrial shed, eaves, *Ansys*, pressure coefficient, height-width ratios, wind directions.

Received: February 24, 2023. Revised: December 13, 2023. Accepted: February 16, 2024. Published: March 12, 2024.

1 Introduction

The use of CFD tools in the study of wind effects has proven to be a viable alternative in recent decades for obtaining data regarding the pressure distribution on the roof in low-rise buildings, allowing the analysis of the various geometric parameters that influence wind loads in this type of building. Some aspects, for instance, height, width, and wind direction, can significantly alter the magnitude of pressure on the roof of a low-rise building, [1]. However, the number of studies of wind loads on curved free roofs is relatively limited, [2], [3].

Recently, some studies have explored the effects generated using the curved eave aspect and, despite the difficulties in making these models, measured wind pressure in wind tunnel experiments, [3], [4].

In this way, [5], reviewed the information available in the open literature about the wind loads on cladded buildings with vaulted roofs, including some significant studies written in Portuguese that are not readily accessible, with the CIRSOC 102 treatment then compared with state-of-the-art results. The authors listed the need to update the code and suggested possible criteria and values for future research.

Using wind tunnel experiments, [6], examined wind pressure characteristics at the rounded edges and, for flat roofs with rounded leading edges, suctions induced by separation bubble and conical vortices increased near the chamfer, decreased beneath the vortices, and invariant far from the principal edge.

Using a wind tunnel experiment and a computational fluid dynamics (CFD) analysis, [7], investigated the fundamental characteristics of wind loading on curved roofs and discussed the effects of rise-to-span ratio, length-to-span ratio, and wind direction on the wind pressure and force coefficients on the roof. The results indicated that the rise-to-span ratio affects the flow and the resulting wind pressures on the roof, and the effect of the length-to-span ratio is relatively small.

Therefore, this work aims to produce data regarding the behavior of pressure coefficients for wind incidents at 45° and 90° in three curved eave models with different height-width relationships.

2 Methodology

In this work, for geometries and simulations, the *Autodesk AutoCAD* and *Ansys Workbench 2023 R2*

software were used, respectively. The solver used to solve the equations was the CFX code.

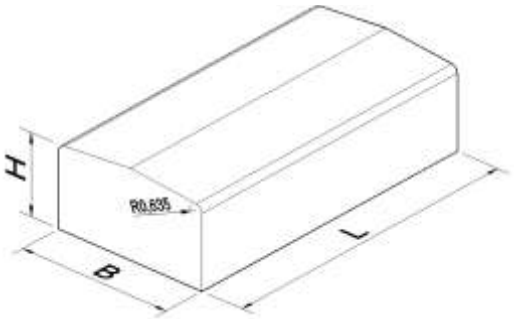

Fig. 1: Geometric configuration

Table 1. Geometric parameters of the models.

Model	Dimensions					Ratios	
	Width (B) [m]	Length (L) [m]	Hight (H) [m]	Eave radius (R) [mm]	Roof Slope (Degree)	H/B	L/B
1	15.00	30.00	7.50	635	5	0.5	2
2	12.50	30.00	12.50	635	5	1.0	2.4
3	10.00	30.00	15.00	635	5	1.5	3

The geometric model chosen was a rectangular shed whose dimensions, including height, were varied (Figure 1). The building also had curved eaves, with a fixed radius of curvature of 635 mm (like those evaluated in [2] and [8]). Furthermore, the building's roof had a fixed slope of 5º in both models (Table 1). The control volume adopted had boundaries 5H away from the front and side facades, the maximum height of the area of interest, and 15H from the rear facade, [9]. In all directions, a sub-domain spaced H/2 for local refinement was adopted.

The unstructured mesh was composed of tetrahedra and has four refinement levels. The first was controlling the size of elements in the fluid domain. The second is control of the sub-domain. The third refers to the facade elements, and finally, the fourth level is the refinement of the eaves and roof elements. The element size adopted was half of the previous level.

The quality of the meshes was analyzed using three parameters: the aspect ratio, the skewness, and the orthogonal quality. For three-dimensional elements, the aspect ratio is the relationship between the radius of the circles circumscribed and inscribed in the base geometry, which, in our specific case, refers to triangles. The skewness indicates the proximity of the cells or faces of the mesh to the ideal geometry, such as a tetrahedron, with recommended values between 0 and 0.5. Additionally, the orthogonal quality metric evaluates the orthogonality of the element, with recommended values approaching 1.0, [10].

The *Power Law approximatio*n was used to incident wind profile, given by:

$$\frac{U_z}{U_{ref}} = \left(\frac{Z}{Z_{ref}}\right)^{\alpha}$$

where U_z is the wind speed (in meters per second) at height Z (in meters), and U_{ref} is the pre-established wind speed at a reference height Z_{ref}. The exponent α is an empirically derived coefficient that varies depending on the terrain roughness and the time interval. Also, α=0.16 representing open terrain with high grass was adopted.

Considering the recommendations of [11] defined the High-Resolution schemes (including additional turbulence equations) since high orders of discretization of the advective terms of the equations solved in the model can improve the accuracy of the results.

The *RNG K-EPSILON* model - widely used in applications such as those analyzed here - was employed to simulate the turbulent effects of the flow. The simulation stopping criterion was the RMS Residual equal to 10E-4, sufficient for many engineering cases, [12].

The results were analyzed using external pressure coefficients (*Cpe*), a dimensionless parameter dependent on the difference in external pressure coefficient (Δp), and dynamic pressure (q) using the expression $Cpe=\Delta p/q$.

In the *Cpe* contour maps, the hot colors represent overpressures (*Cpe*>0), and cold colors represent suctions (*Cpe*<0).

Finally, Table 2 shows the rest of the boundary conditions adopted.

Table 2. Boundary conditions and non-dimensional parameters

Condition	Parameters
Method of mesh	Tetrahedron
Capture curvature and proximity	On
Reference pressure	101325 [Pa]
Air temperature	25º [C]
Turbulence intensity	Medium (5%)
Flow regime	Subsonic
Inlet	$U/U_{ref} = (Z/Z_{ref})^{\alpha}$
α	0.16
Z_{ref}	40 [m] (*Application 1*)
	10 [m] (*Application 2*)
U_{ref}	33 [m/s] (*Application 1*)
	30 [m/s] (*Application 2*)
Relative pressure of outlet	0 [Pa]
Wall - Ground	Rough wall
Model wall roughness	Smooth wall
Roughness	0.01 [m]
Advection scheme	High resolution
Turbulence numeric	High resolution
Minimum number of iterations	100
Maximum number of iterations	300

3 Numerical Results

Application 1 (*validation*): To validate the methodology, two low-rise building models with a flat roof and rounded leading edge were evaluated, [6]. The buildings had dimensions of 120x120x40 m (BxWxH) and edge rounding radii of 5.00 m and 7.00 m.

Figure 2 shows the representation of the model, and Table 3 brings together the details of each work.

Here, the naming of the models is the same as in the original work, *FM2* and *FM3* models.

Qualitatively, based on the *Cpe* contours, it was possible to note, in both cases, the similarity of the models with the original work (Figure 3).

Due to the detachment of the flow, the most intense zones appeared on the windward edges, although, in the present work, they occupy a larger region of the coverage. One can also notice a large central area with uniformly distributed *Cpe* values.

Quantitatively, the *T-test* was used to evaluate a statistically significant difference between the means of two *Cpe* samples.

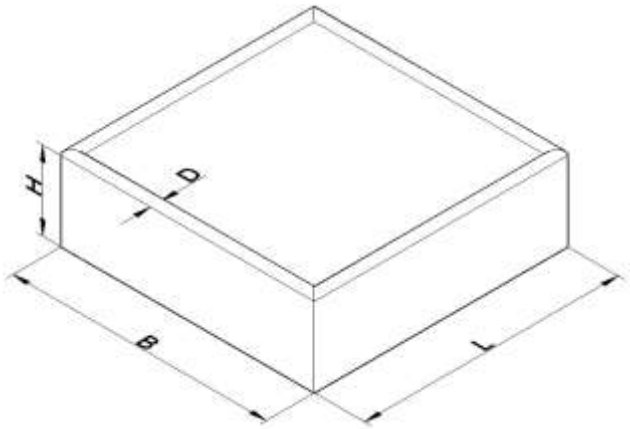

Fig. 2: Representation of the models analyzed in validation

Thus, were extracted data from 10 points (Table 4) along the line "X" illustrated in Figure 4. Furthermore, an *F-test* was applied to define whether the data variances were supposedly equivalent or different. For the *FM2* model, considering the null hypothesis (H_0) that the means are not statistically significant, assuming two samples with equal variances, two-tailed distribution, and significance α' = 0.05, and using *Microsoft Excel* software obtained a p-value = 0.2670.

As p-value > α', we do not reject the null hypothesis (H_0) and consider the difference between the means in the *Cpe* values insignificant. Similarly, for the *FM3* model, however, assuming different variances, we obtain a *p-value* = 0.0930. Also, as *p-value* > α', we do not reject the *null hypothesis* (H_0), considering insignificant differences between the means. Therefore, the methodology is appropriate to produce results accurate to reality.

Application 2 (*variation in width, length, and height of buildings with curved eaves*): Table 5 shows the results of the simulations referring to Models 1, 2, and 3 regarding the variation in width, length, and height of the buildings. For the three models, the high suction was more pronounced in the 90º wind in the region of approximately 0.00% of the span, as shown in Figure 5(a), Figure 6, Figure 7 and Figure 8. In addition, there was an inversion in the pressure distribution from ~60.00% of the span, in which the magnitude of the pressures became maximum in the 45º wind configuration. In Figure 5(d), the velocity contour showed that the wind accelerated in the leeward region, causing a higher velocity. This unexpected behavior is responsible for the higher magnitude of the suctions in the 45º configuration.

In Models 2 and 3 with the wind at 45º, the external pressure coefficient values are close, especially at ~0.00% of the span (Figure 8 (b) and Figure 8(c)). This behavior was similar for the 90º wind, nonetheless, only from ~50.00% of the span.

However, the results showed that the values of the pressure coefficients in both wind directions were closer in this model than in model 1.
In all Models with the wind at 45º, it was noted in the vicinity of the leeward an increase in suction, intensified with the h/b ratio reduction. Also, with the increase in the height-to-width ratio, a considerable growth in suctions at ~0.00% of the span was noted.

Table 3. Model information summary

Model	**Dimensions**				**Angle of attack (degree)**
	Width (B) [m]	**Length (L) [m]**	**Hight (H) [m]**	**Edge diameter (D) [m]**	
FM2 (*present work*)	120.00	120.00	40.00	5.00	45
FM3 (*present work*)	120.00	120.00	40.00	7.00	45
Mesh data					
Model	**Nodes**	**Elements**	**Aspect ratio (average)**	**Skewness (average)**	**Orthogonal quality (average)**
FM2 (*present work*)	218393	1205800	1.9687	0.27433	0.72459
FM3 (*present work*)	186367	1020871	1.9575	0.27041	0.72853

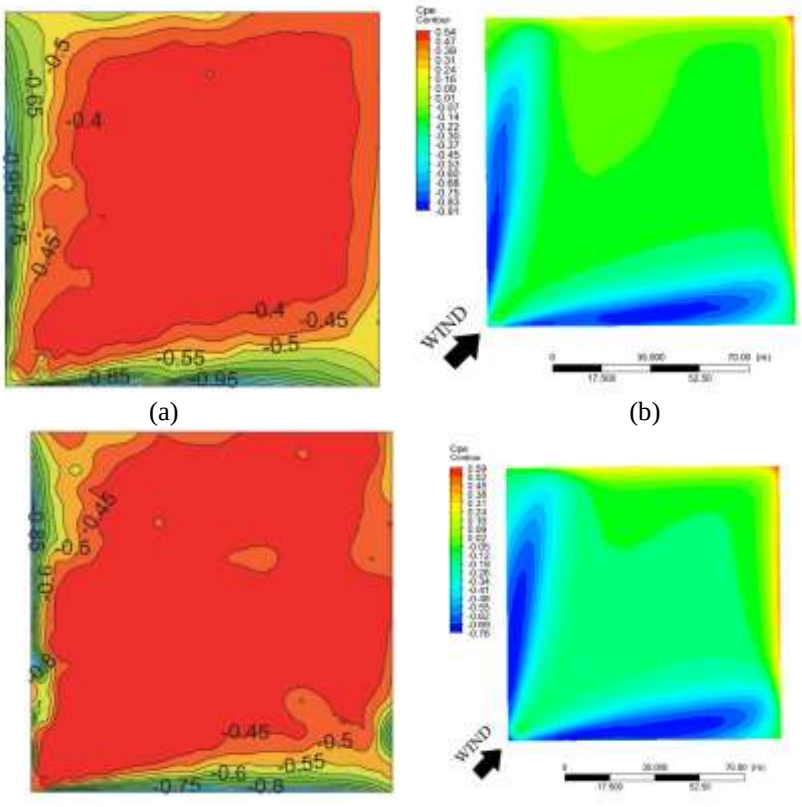

(a) (b) (c) (d)

Fig. 3: Top view of the *Cpe* contour map on the roofs of models (a) FM2 [4], (b) FM2 (present work), (c) FM3 [4] and (d) FM3 (present work) (the map does not include the results of the leading edges)

Table 4. Data for *T-test* and *F-test* of FM2 and FM3 models.

Model	**Points**	**1**	**2**	**3**	**4**	**5**	**6**	**7**	**8**	**9**	**10**
FM2 [6]	***Cpe***	0.729	0.519	0.411	0.378	0.360	0.348	0.338	0.341	0.347	0.345
FM2 (*present work*)		0.790	0.565	0.410	0.300	0.260	0.200	0.190	0.180	0.175	0.170
FM3 [6]		0.614	0.484	0.419	0.405	0.403	0.395	0.394	0.396	0.379	0.350
FM3 (*present work*)		0.710	0.560	0.400	0.280	0.225	0.185	0.180	0.175	0.170	0.165

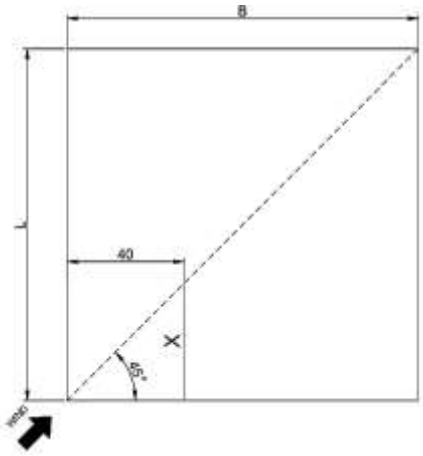

Fig. 4: Data extraction region for *T-test* and *F-test*, according to the format originally proposed and evaluated in [4]

Table 5. Mesh results for models 1, 2, and 3

Mesh data						
Model	**Wind direction (degree)**	**Nodes**	**Elements**	**Aspect ratio (average)**	**Skewness (average)**	**Orthogonal quality (average)**
1	45	425854	2334618	1.8950	0.24821	0.75067
	90	416230	2287943	1.8917	0.24696	0.75192
2	45	411527	2258825	1.9128	0.25534	0.74348
	90	400045	2195354	1.9153	0.25614	0.74267
3	45	401910	2213536	1.9220	0.25780	0.74115
	90	388571	2139797	1.9223	0.25798	0.74098

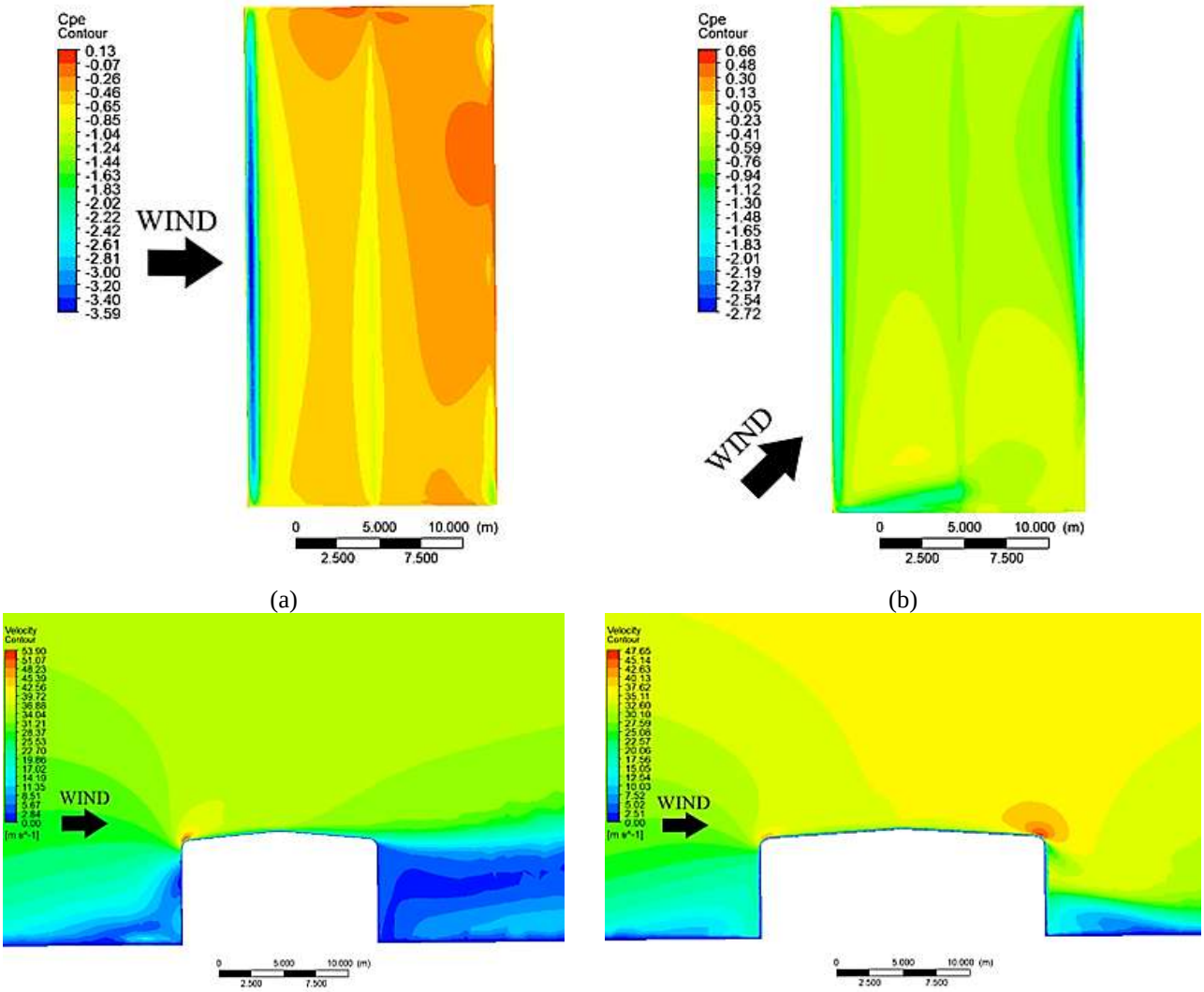

Fig. 5: Wind pressure coefficients across the roof at (a) 90º and (b) 45º respectively and the velocity contour with the wind at (c) 90º and (d) 45º for model 1

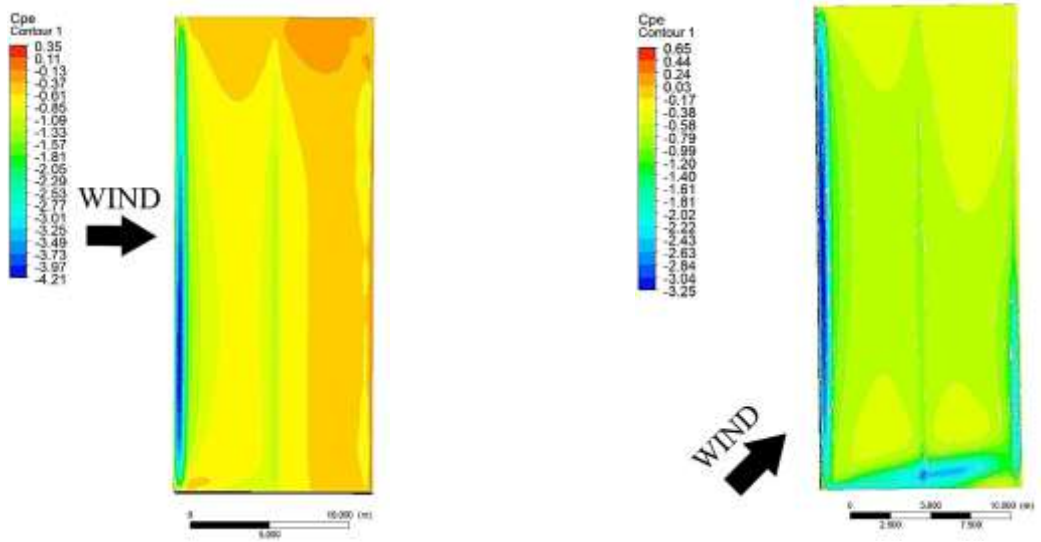

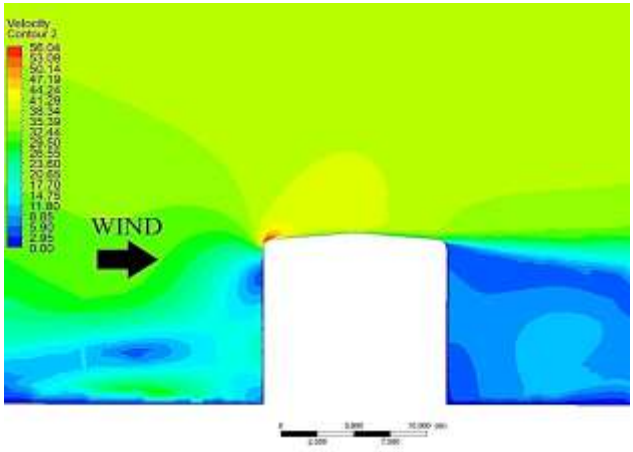

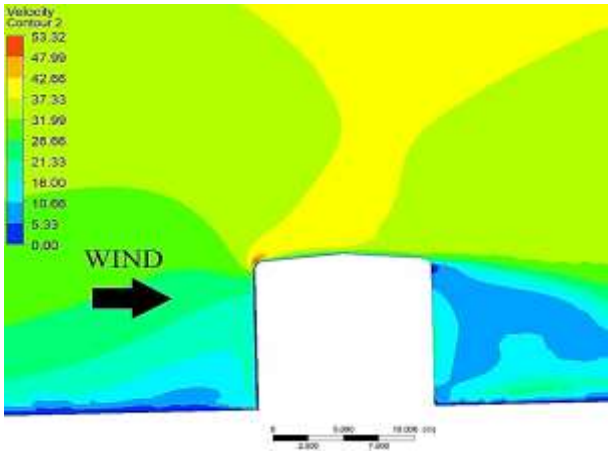

(c) (d)

Fig. 6: Wind pressure coefficients across the roof at (a) 90º and (b) 45º respectively and the velocity contour with the wind at (c) 90º and (d) 45º for model 2

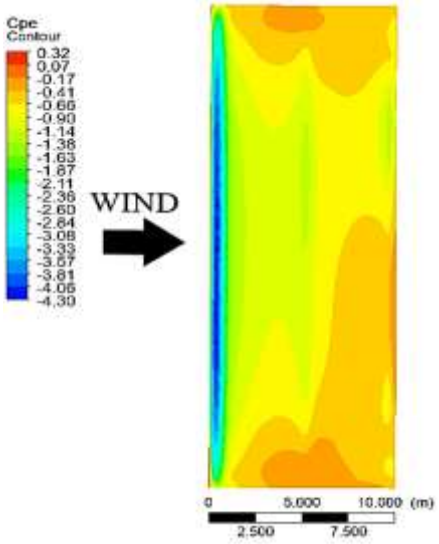

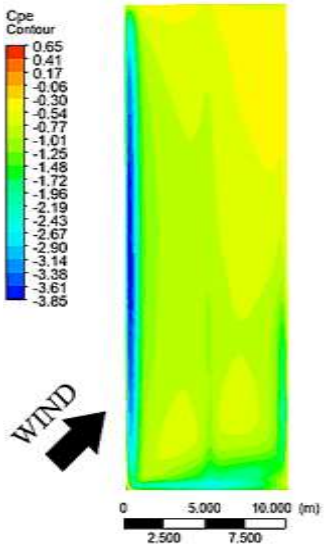

(a) (b)

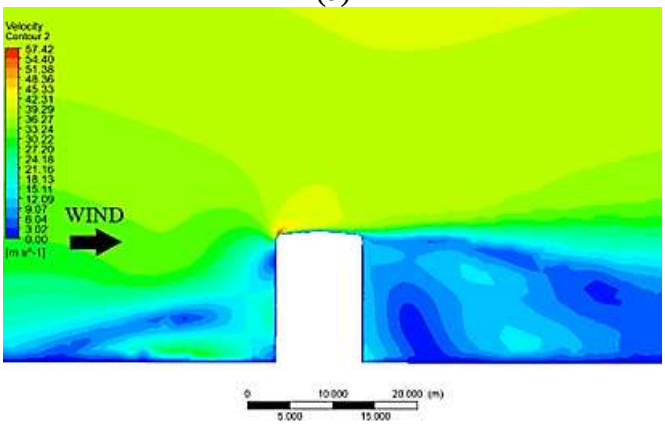

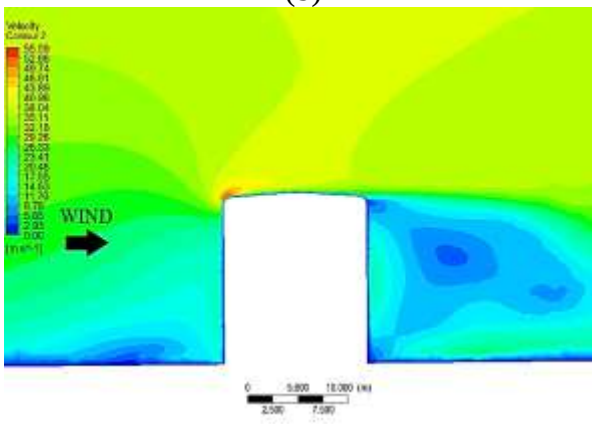

(c) (d)

Fig. 7: Wind pressure coefficients across the roof at (a) 90º and (b) 45º respectively and the velocity contour with the wind at (c) 90º and (d) 45º for model 3

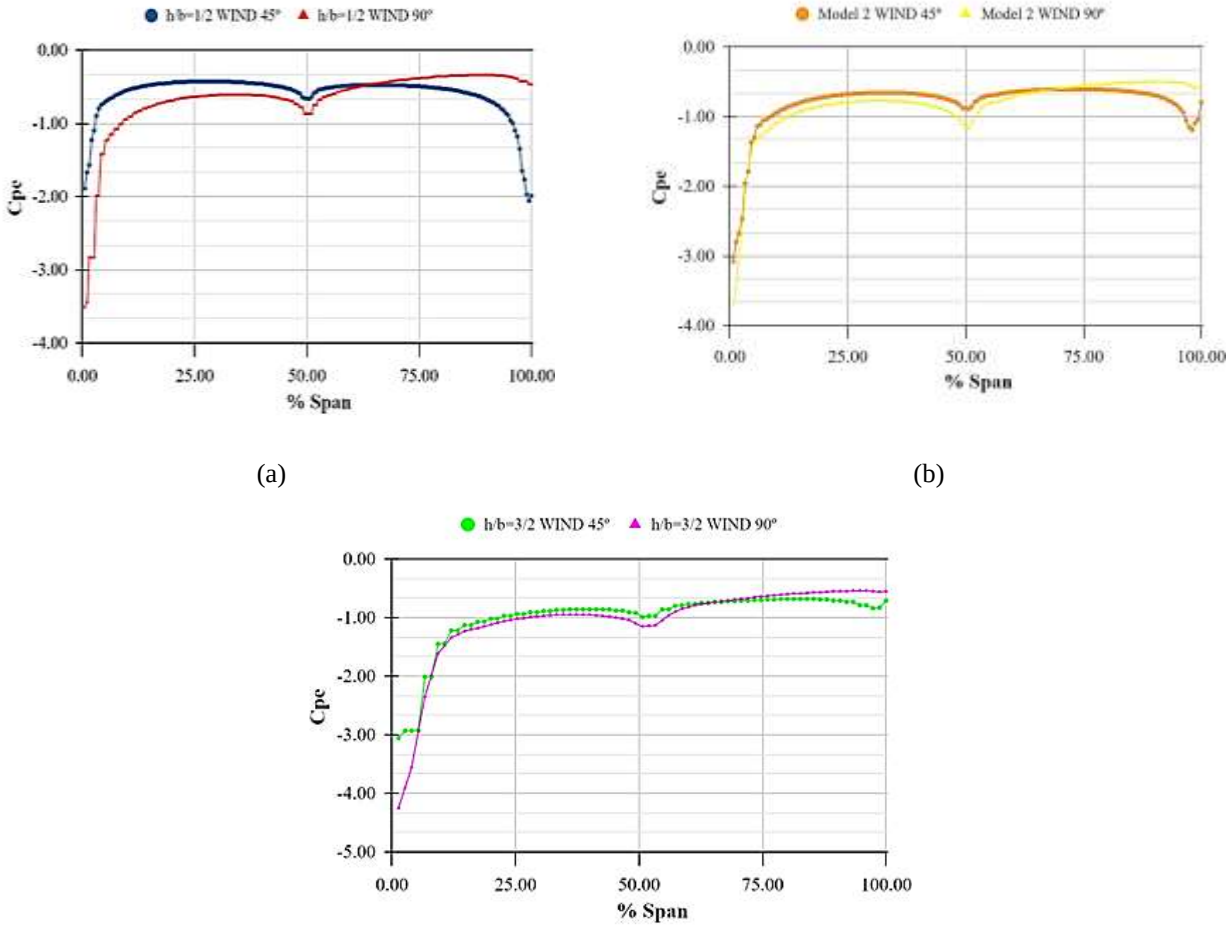

Fig. 8: Pressure coefficients plotted normal to the ridge for (a) Model 1, (b) Model 2, and (b) Model 3, respectively

4 Conclusions

In this work, the pressure coefficients on the roof of three models with curved eaves and different height-to-width ratios were generated for two wind directions (90º and 45º) using *Ansys Workbench* software.

The results showed similar behavior for the pressure distribution in models when analyzing both wind directions: the magnitude of the pressures increased with the wind at 90º up to approximately 60.00% of the span; for the wind at 45º, the pressures were higher in the remaining region. In this way, the leeward region with the wind at 90º configuration can be neglected. For wind at 45º, attention should be paid to the windward and leeward regions, since for height-width relations less than 1.5, the pressures intensify in the leeward direction for height-width relations less than 1.5.

Furthermore, the increase in the height-width ratio was more harmful to regions close to the windward eaves with a 90º wind configuration.

In the results obtained via CFD, the regions with the most intense winds have the highest pressure coefficient values, as discussed in Fluid Mechanics, and the leeward region in 90º configurations is less damaging than the windward region, according to [3].

Given the above, the work carried out contributes to the formation of data in the literature regarding the analysis of the influence of curved eaves on wind loads in low-rise buildings. In this way, future studies will be able to analyze the behaviour of external pressure coefficients for different height-width relationships with changes in the slope and radius of the eaves. In addition, other types of relationships may be considered, such as height-length and length-width.

References:

[1] R. P. Hoxey, A. P. Roberstson, B. Basara and B. Younis, Geometric parameters that affect wind loads on low-rise buildings: full-scale and CFD experiments, *Journal of Wind Engineering and Industrial Aerodynamics*, Vol. 50, 1993, pp. 243-252.

[2] A. P. Robertson, Effect of eaves detail on wind pressures over an industrial building,

Journal of Wind Engineering and Industrial Aerodynamics, Vol. 38, 1991, pp. 325-333.

[3] W. Ding and Y. Uematsu, Discussion of Design Wind Loads on a Vaulted Free Roof, *Wind*, Vol. 2, 2022, pp. 479–494.

[4] B. Natalini and M. Natalini, Wind loads on buildings with vaulted roofs and side walls – A review, *Journal of Wind Engineering and Industrial Aerodynamics*, Vol. 161, 2017, pp. 9-16.

[5] B. Natalini, J. O. Marighetti and M. B. Natalini, Wind tunnel modeling of mean pressures on planar canopy roof. *Journal of Wind Engineering and Industrial Aerodynamics*, Vol. 90, 2002, pp. 427–439.

[6] X. Dong, J. Ding and C. Jiao, Wind loads on flat roofs of low-rise buildings with rounded leading edge, Journal of the Chinese Institute of Engineers, DOI: 10.1080/02533839.2018.1559766, 2019.

[7] W. Ding, Y. Uematsu and L. Wen, Fundamental Characteristics of Wind Loading on Vaulted-Free Roofs. *Wind*, Vol. 3, 2023, pp. 394–417.

[8] G. S. Teixeira and M. D. Campos, Numerical study on wind pressures caused by the variation of the rounding radii of the industrial shed eaves, *Engineering World*, Vol. 5, 2023, p. 10-16.

[9] J. Franke, A. Hellsten, H. Schlünzen and B. Carissimo, *Best practice guide for the CFD simulation of flows in the urban environment, COST Action 732: Quality assurance and improvement of microscale meteorological models.* Hamburg: COST Office, 2007.

[10] ANSYS, *CFX-Solver Theory Guide Ansys*, Canonsburg, 2009.

[11] J. Franke, C. Hirsch, A. G. Jensen, H. W. Krüs, M. Schatzmann, P. S. Westbury, S. D. Miles, J. A. Wisse and N. G. Wright, *Recommendations on the use of CFD in predicting pedestrian wind environment, COST Action C14: Impact of Wind and Storms on City Life and Built Environment. Hamburg*, COST Office, 2004.

[12] ANSYS, *CFX-Solver Modeling Guide Ansys*, Canonsburg, 2009.

Contribution of Individual Authors to the Creation of a Scientific Article (Ghostwriting Policy)

Guilherme Teixeira was responsible for the methodology, carrying out the simulation, and writing the validation. Leonardo Teodoro wrote the results and conclusions. Marco Campos carried out the conceptualization, review, and editing.

Sources of Funding for Research Presented in a Scientific Article or Scientific Article Itself

The present work was partially supported by Federal University of Mato Grosso.

Conflict of Interest

The authors have no conflicts of interest to declare.

Creative Commons Attribution License 4.0 (Attribution 4.0 International, CC BY 4.0)

This article is published under the terms of the Creative Commons Attribution License 4.0
https://creativecommons.org/licenses/by/4.0/deed.en_US